Synthesis and characterization of ZnO nanorods via hydrothermal route for wastewater recycling

B.. Ahmad [a], M. Irfan [a,*], M. I. Khan [b], M. Atif [c], I. Ahmad [d], A. Sharif [e]
[a] *Department of Physics, University of Okara, 3600, Okara, Pakistan*
[b] *Department of Physics, University of Lahore, 53700, Pakistan*
[c] *Department of Physics and Astronomy, college of science, King Saud University, Riyadh 11451, Saudi Arabia*
[d] *Department of Physics and Astronomy, Texas Tech University, Lubbock, TX 79409, USA.*
[e] *Department of Environmental Sciences, University of Lahore, 53700, Pakistan*

In this work, highly efficient ZnO nanorods (NRs) were prepared using an easy and cost-effective hydrothermal process. The Synthesized ZnO NR have been analyzed for their structure, morphology, and optical characteristics using X-ray diffraction (XRD), field emission scanning electron microscopy (FESEM), Fourier Transform Infrared (FTIR), and ultraviolet-visible (UV-visible) spectroscopy, respectively. Additionally, a test is conducted on the ZnO nanorod's photocatalytic efficiency towards the degradation of certain dyes, Methylene Blue (MB) and Methyl Orange (MO). The FESEM investigation revealed that the ZnO nanostructures show nanorods with varying diameters (needle-like shape) with an estimated size of (10 to 20) µm. According to the XRD examination, the NRs had a hexagonal-shaped wurtzite pattern, exhibiting an average crystallite diameter of about 50 nm. FTIR spectra confirmed that functional groups from the substance being extracted were present in the ZnO NRs. The band-gap value of 3.37 eV was determined through the TAUC plot model from the ultraviolet-visible spectrum data. In the presence of as-synthesized ZnO NRs, the MO dye degraded by 100 percent in 46 minutes, but the MB dye significantly degraded by approximately 100 % in 20 minutes with high degradation rate constants k_{MO} = 0.086 min^{-1} and k_{MB} = 0.180 min^{-1}, respectively.

(Received August 1, 2024; Accepted November 4, 2024)

Keywords: Hydrothermal synthesis, ZnO nanorods, Photocatalysis, Methylene blue, Methyl orange

1. Introduction

Numerous industries and technologies, including the fields of transportation, medicine, food preservation, energy, and the environment, have benefited greatly from nanotechnology, which has even completely revolutionized some of them [1-3]. Organic dyes are among the many various sorts of waste produced by industries worldwide [4,5]. This is because organic dyes are difficult to biodegrade and hinder sunlight from penetrating water, which hinders photosynthesis. Such dyes are utilized in the food, skincare products, paper, packaging, textiles, and pharmaceutical sectors [6]. The greatest amounts of water contamination are caused by the effluents drained by these industries especially the textile sector where dyes are used as a major component [4,7-9]. Global literature indicates that each year, 2.8 x 10^4 tons of synthetic dyes are wasted due to industrial discharge into the environment [10,11]. It is crucial to remove chemical dyes like methyl orange (MO), Tartrazine, methylene blue (MB), congo red (CR) as a cationic, and malachite green (MG) as an anionic dye from water resources because they can cause several problems, including respiratory tract infections, skin conditions, and eye irritation [12,13].

* Corresponding author: m.irfan6570@gmail.com
https://doi.org/10.15251/JOR.2024.206.779

Various methods are employed to remove organic dyes, contaminants, and non-biodegradable materials from water, including ozonation, ion exchange, reductive degradation, adsorption, Fenton reaction, and microbiological operations [14-17]. Among these techniques, the most effective method for eliminating pollutants is nanomaterials-based photocatalysis, an easy, cheap approach that produces no harmful byproducts [18][19]. Heterogeneous photocatalysis using ZnO in the sunshine is a promising technique for the purification of drinking water and wastewater treatments. Using this technique, various UV and visible light wavelengths stimulate the nanomaterials based on the energy band gap [20-23]. Through a photocatalytic redox process, the activated nanomaterials break down the different chemical and microbiological contaminants in water [24, 25]. The viability of semiconductor nanostructures, such as $BiFeO_3$, WO_3, SrO_2, CeO_2, TiO_2, CdS, Fe_2O_3, ZnO, etc., in photocatalysis has been the subject of numerous research recently. Among all the above semiconductor oxides, Zinc oxide (ZnO) with a wide band gap (3.37 eV) at room temperature with a high electron mobility rate (200 – 300 $cm^2V^{-1}s^{-1}$), high thermal stability, non-toxic nature, strong oxidizing agent and easily available in the earth crust has received great attention in the environmental remediation processes [26-28]. Al-Gharibi et al. created a composite of Ag-doped ZnO nanorods (ZnO-NRs), and they utilized photocatalysis facilitated by sunlight to break down 92% of the contaminated paracetamol in just four hours [29]. Many attempts have been made by a variety of researchers to use ZnO semiconductor / metal-doped heterostructure to boost charge transfer (CT) by reducing electron-hole recombination [20–22, 30]. These nanostructures can be synthesized using a variety of methods, including microwave-assisted synthesis [31], sol-gel process [32, 33], sputtering [34], laser ablation [35], radiofrequency [36], hydrothermal approach [37], electro-deposition [38], and others [39-42]. Among various preparation techniques, the synthesis of semiconductors via hydrothermal approach offers a novel way to achieve high-efficiency photocatalysts with control particle size because it improves the interfacial CT to adsorbed organics and realizes more efficient charge separation [43-46].

In this study, ZnO NRs have been produced using the hydrothermal method to test the photocatalytic activity of dyes Methylene Blue (MB) and Methylene Orange (MO), which are widely found in wastewater. The variation in the thickness (about 50 nm) and length of the synthesized nanorods in the 500 nm range can result in a larger surface area, which in turn provides more active sites for photocatalytic reactions. The wider surface area significantly improves the contact between the photocatalyst and the targeted waste products, resulting in higher photocatalytic efficiency. This research contributes to the growing body of knowledge in sustainable water treatment, offering potential solutions to the challenges posed by organic dye contamination in our water resources.

2. Materials and methods

2.1. Materials

$Zn(NO_3)_2$•$6H_2O$ (0.02M), and NH_4OH (with 33% NH_3) were obtained from company MERCK (E. Merck, Darmstadt, F. R. Germany). Methanol (99.8%), Hydrogen peroxide (34.5-36.5%), and iso-propanol were obtained from Sigmą-Aldrich, Germany. Zn sheets (99.9%) were purchased from SinopharmmChemical Reagent Co. Ltd. Heterocyclic fragrant colors methylene blue (MB) and a color dye methylene orange (MO) were purchased from ALFA, AESAR. Various synthetic materials were evaluated critically and used as provided. De-ionized water was used for all of the manufacturing assessments.

2.2. Prepration of ZnO nanorodes

A measured quantity of Aqueous solution of (0.02M) $Zn(NO_3)_2$•($6H_2O$) in 60 ml (0.714gm/120ml) of distilled water was prepared in a beaker and placed on a magnetic stirrer for stirring. The pH of the solution was checked with pH paper before mixing NH_4OH sol (with 33% NH_3) which was 6pH. The 60 ml sol was divided into three beakers in equal quantities (20 ml). Now NH_4OH sol (with 33% NH_3) was dropwise turned by turn and slowly into each beaker containing (0.02M) $Zn(NO_3)_2$•($6H_2O$) stirring solution to prepare three different samples with the same pH values of 10.5pH. It was noticed that by dropping NH_4OH into the $Zn(NO_3)_2$ ($6H_2O$) precursor

solution its color turned to dim/light blue which disappeared after some time. The stirred solution was poured into three different Teflon-lined autoclaves. The substrates (Zn metallic sheets), with polished surface upward, were carefully inserted into these autoclaves.

2.3. Heating, drying, extraction and calcination

The autoclave was closed firmly and placed into the incubator at 60 °C for 6 hr. After the reaction was completed, the product (Zn substrates) was taken out of the autoclave at room temperature, washed three times with ethanol, and incubated at 70 °C for 10 hr. ZnO synthesized on Zinc substrates was received and saved for further heat treatments. The hydrothermally synthesized products were calcined in a furnace at 650 °C for 4 hr. Centrifuging the product at a rate of 7000 rounds per minute was used to extract it after it had been gradually cleaned with ethanol and water reagents to remove any deposits and pollutants.

2.4. ZnO nanorods characterization

SEM analysis was conducted using a PHILIP XL-30 at 30 kV to study the shape and structure of the ZnO nanorods. The ingredient composition was performed utilizing an EDS system coupled to a SEM machine. X-ray diffraction (XRD) was used to investigate the structure of crystals and phase behavior of ZnO Nanorods. A Siemens D5000 diffractometer with CuKα wavelengths the radiation (λ = 1.540598 Å) was applied to scan the various graphs at ambient temperature. We utilized an FTIR apparatus, Thermo Scientific iS50 FTIR Spectrometer, to investigate the structure of the ZnO NR's. It has a measurement range of 400 to 4000 Cm^{-1}. To conduct UV–visible spectroscopy, the nanopowder obtained from each reaction was carefully re-suspended in sterile de-ionized water. An Ava Spec-2048TEC spectroscopy device was employed to conduct spectrum scanning. It operates within the wavelength range of 190-800 nm and has a scanning speed of 600 nm/s.

2.5. Photocatalytic activity

ZnO nanorods were used as a catalyst in a fluid medium to break down MO and MB when exposed to intense (UV) light. The experiments followed mellow mixing and were executed at ambient temperature. To spread the photoreaction Heat is produced via restricted convection by using an electric fan. For optimal adsorption, 30 mg of ZnO photocatalysts were added with 60 ml of a 15 µM concentration of each organic dye. As UV light, a 300-watt Xenon generator (Xenon-Bulb Beijing Trusttech PLS-SXE300) was used. The reaction chamber was situated approximately thirty centimeters (30 cm) from the light source. To estimate absorbance, 3-5 milliliters of the irradiated solution were taken out from the vessel.

3. Results and discussion

3.1. X-ray diffraction (XRD) analysis

X-ray diffraction (XRD) assessment is an approach frequently used to investigate the crystal structure of materials. The arrangement of atoms in a crystal lattice is revealed by the XRD pattern. The XRD spectra of hexagonal wurtzite pure ZnO Nanorods with high crystallinity are presented in Figure-1 with (JCPDS #01-087-0713). Figure-1 depicts Some significant peaks that correspond to the pure ZnO nanorods with crystal planes (100), (002), (101), (102), (110), (103), (200), (112), (201), (004), (203) having diffraction angles 2θ at 31.78°, 34.30°, 36.35°, 47.52°, 56.47°, 62.66°, 67.95°, 70.15°, 72.52°, 72.67° and 90°, respectively. Additionally, the pattern also shows some peaks of another phase. These are attributable to zinc considering the sample was produced on a zinc sheet and, following washing and drying, as exactly in the same form was sent for XRD examination. By employing the Debye-Scherrer formula, the average crystallite size was determined as follows:

$$D = \frac{K\lambda}{\beta \mathrm{Cos}\theta} \tag{1}$$

Here, the average crystallite size is represented by D, while λ denotes the wavelength for Cu Kα radiation at 1.5406 Å. The full width at half maximum (in radians) associated with the (101) plane is indicated by β, and θ refers to the Bragg angle measured in degrees. The average crystal size was found to be around 29.58 nm, and the subsequent formula was employed to compute the interplanar spacing,

$$d = \frac{n\lambda}{2Sin\theta} \tag{2}$$

Here, within this context, d stands for the interplanar spacing, n for the order, λ for the wavelength of 0.15406 nm (CuK), and θ for the diffraction angle. The average spacing was found to be around 1.76 Å.

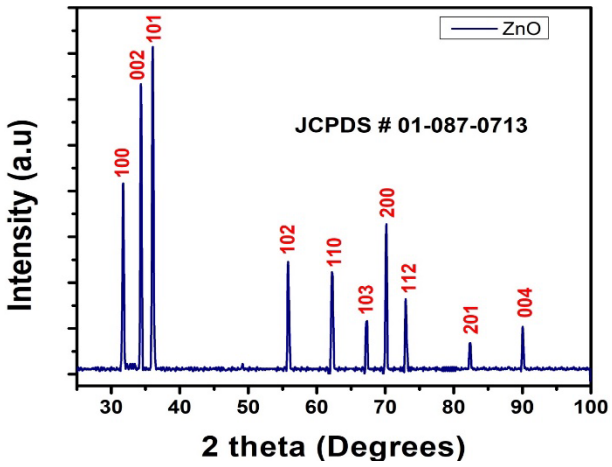

Fig. 1. XRD pattern of ZnO nanorods.

Table 1. Detailed physicochemical properties ZnO Nanorods.

Material	Crystallite size (nm)	Micro strain (10^{-3})	Dislocation density $(nm)^{-2}$ x 10^3	Crystallinity (%)	Eg (eV)	Lattice Constant	
						|a|	|c|
ZnO	31.64	0.84	1.04	77.58	3.37	0.44	3.88

3.2. FTIR analysis

The FTIR analysis revealed the presence of several functional groups on the surface of the synthesized material. Figure 2 displays the ZnO nanorod's FTIR spectrum. The distinct functional groups present in the zinc oxide nanorods are represented by their corresponding peaks in the spectra [50,51]. The FITR spectra included the characteristic peaks observed in ZnO nanorods at 3441, 2940, 1615, 1386, 1101, 1033, 625 and 454 cm^{-1}. The broadband noted at 3441 cm^{-1} arises from the stretching vibration associated with the O-H functional group [52]. The stretching vibrations of C-H bonds cause the sharp band at 2940 cm^{-1} and carbonyl ester (C=O) is responsible for the peak observed at 1615 cm^{-1} [53,54]. The observed peaks at 1101 cm-1 and 1386 cm^{-1} correspond to the in-plane bending or vibration modes associated with primary and secondary alcohols, respectively. The minor peak observed at 1033 cm^{-1} can be ascribed to the stretching mode of aromatic C=C bonds [53]. A vibration band bending O-H is observed at 625 cm^{-1}. The band at 454 cm^{-1} is attributable to Zn-O bond stretching vibrations, which demonstrates the production of the product [55-56].

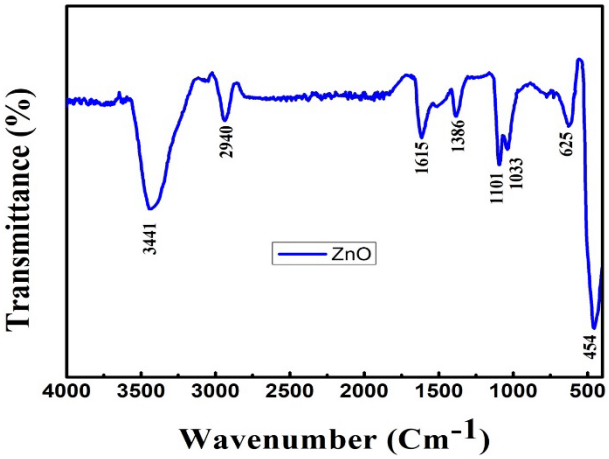

Fig. 2. FTIR spectra of ZnO nanorods.

3.3. UV-Vis spectroscopy

To investigate the optical properties of nanometer-sized particles, an ultraviolet-visible absorption spectroscopy technique was employed [57-58]. The UV–vis absorption curves of ZnO nanorods calcination at 400 ^{0}C for 2hrs are presented in figure (3-a). Analysis of the ultraviolet spectra was performed in the region of 200–800 nm. ZnO is characterized as a direct band-gap semiconductor, having a large band gap that exists between the conduction and valence bands. As a result, the UV-Vis spectrum often displays a wide absorption band within the ultraviolet domain. An electron's jump from the valence to the conduction band creates this absorption band, and its numerical value is utilized to ascertain the band-gap value of ZnO [41]. Based on the absorption spectra and using Tauc's equation, the band gap energy of the sample was evaluated.

$$ahv = A(hv - Eg)^{1/2} \tag{3}$$

The Tauc's plot is presented in Figure (3-b). The direct band gap energy of the ZnO nanorods is determined at 3.37 eV by using eq (1). This wide band gap is important because increased band gap energies improve photocatalytic capabilities and slow down the rate at which electron and hole pairs recombine.

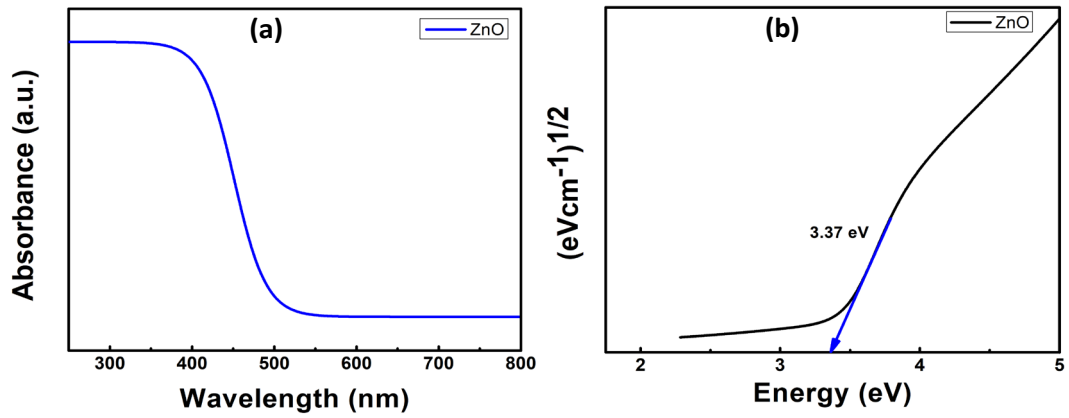

Fig. 3. UVspectra of ZnO nanorods (a) Absorbance (b) Direct band gap.

3.4. SEM

SEM was used to characterize the morphological and structural investigations of the hydrothermally produced ZnO nanorods as shown in Figure 4 (a-c). According to FESEM images, ZnO nanorods with varying thicknesses (with needle-like structures) and lengths in the nanometer range have been created. They are distinctly separated but most of the rods are irregularly piled up on each other as shown in Figure 4 (a-c). Upon close inspection at high magnification, it becomes evident that the length of these rods differs from one another. As observed from the histogram particle size distribution shown in Figure (5-a), their thickness ranges from 10 to 100 nm, with an average diameter of 50 nm and the observed length of the NR is in the range of 500 nm. They have a needle-like shape because they are narrow at one end and thick at the stem. The existing literature [47-49] has reported morphologies that are strikingly comparable to the ones used in this study. The corresponding ZnO nanorod EDS spectrum is shown in Figure (5-b), demonstrating the purity of the product and the percentage of the existing elements. The main peaks are ascribed to Zinc and Oxygen.

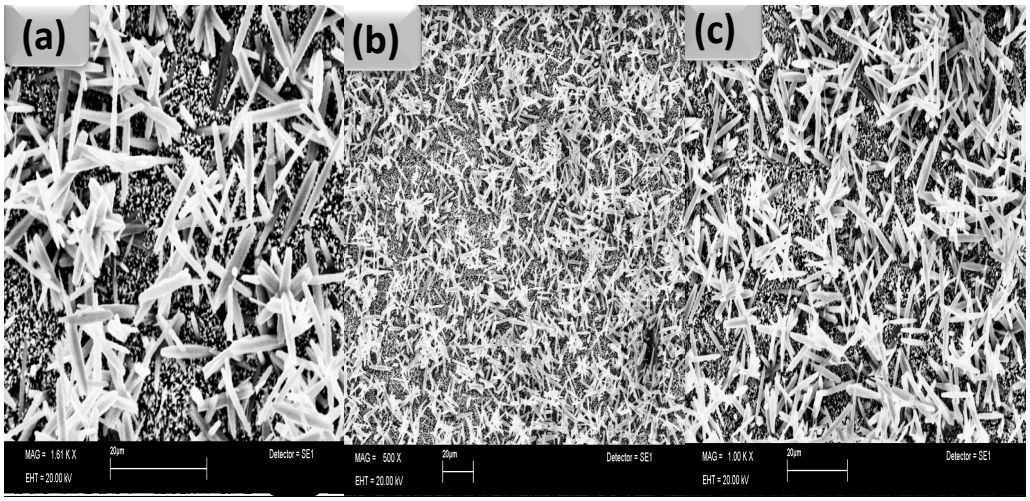

Fig. 4. FESEM images of ZnO nanorods at different magnifications.

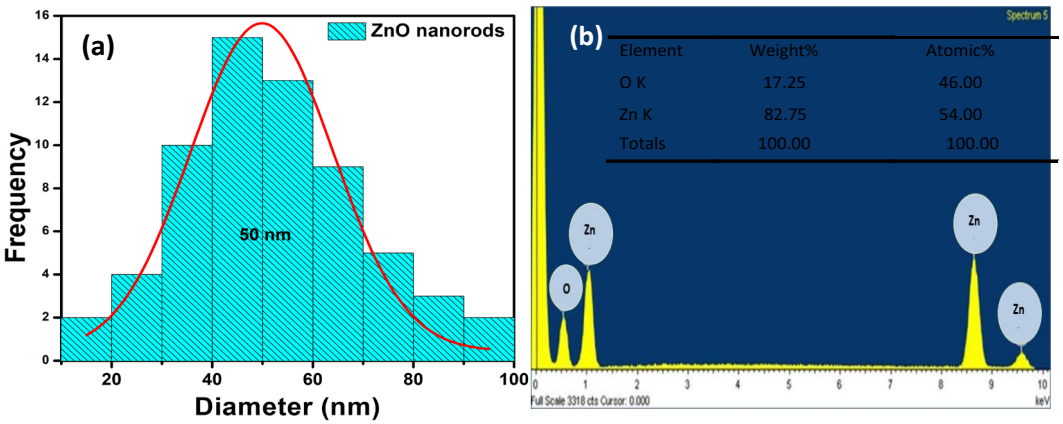

Fig. 5. (a) Histogram distribution of ZnO nanorods diameters (b) EDS spectrum of ZnO with elemental ratio.

3.5. Photocatalytic activity

The photocatalytic activity of ZnO nanorods was studied by exposing them to UV light in the water while contaminating them with Methylene Blue (MB) and methyl orange (MO) dyes.

3.5.1. Methyl Orange degradation

Figure 6 (a) displays the time-varying sequence of wavelengths of absorption that illustrate the room temperature degradation of pure MO combined with the dye's instantaneous mode degradation. It is clear by analyzing the spectra that even after 120 minutes of radiation, the absorbance peaks of the blank MO (in the absence of a catalyst), which are located at about 460 nm, do not exhibit a significant decrease. Figure 6 (b) illustrates the photocatalytic degradation of MO with the addition of ZnO nanorods acting as photo-catalytic materials. The figure illustrates as the UV irradiation exposure period increases, the distinctive peaks of MO in the presence of ZnO nanorods acting as a photocatalyst decrease and subsequently disappear completely after 46 minutes. It has been found that when ZnO nanorods are present as a catalyst, the degradation of MO dye occurs more quickly than the degradation of MO blank when exposed to the same UV light. As a result, the presence of ZnO nanorods as a photocatalyst has increased MO degradation relative to the blank sample, which degrades very little, as shown by the assessment of the kinetics of the reaction shown in Figure 6 (c).

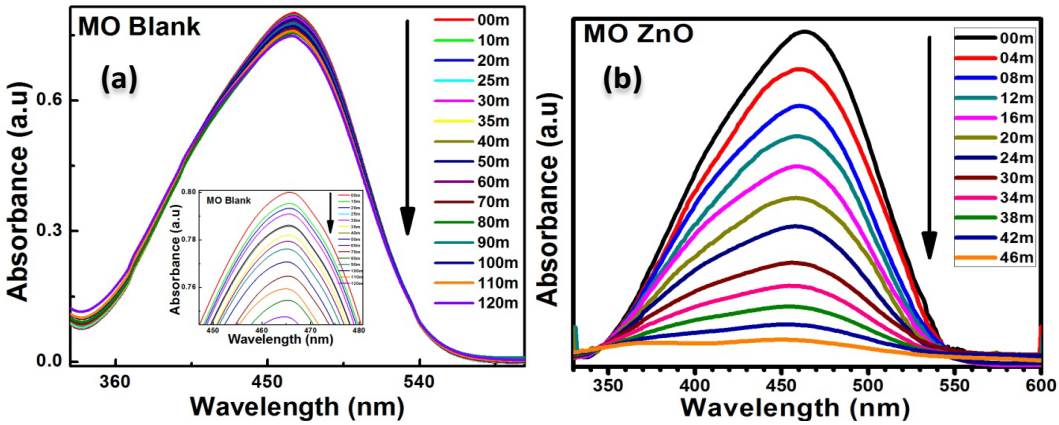

Fig. 6 . UV-Vis spectra of photocatalytic degradation of methyl orange (MO) (a) blank (b) ZnO as a catalyst.

Figure 7 depicts the relationship between MO concentration and UV irradiation period, with C_t and C_0 representing MO concentrations after degradation and at the initial stage, respectively. Figure (7-b) shows a first-order kinetics model for MO degradation, determined by using equation (4).

$$\ln C_0 / C_t = k_{MO} t \quad (4)$$

Where k_{MO} and t are the degradation rate constant and UV light exposure time of MO. The degradation rate constant of MO in the presence of ZnO nanorods (k_2 = 0.086 min-1) was significantly higher than that of MO Blank, indicating 95% quicker degradation of MO.

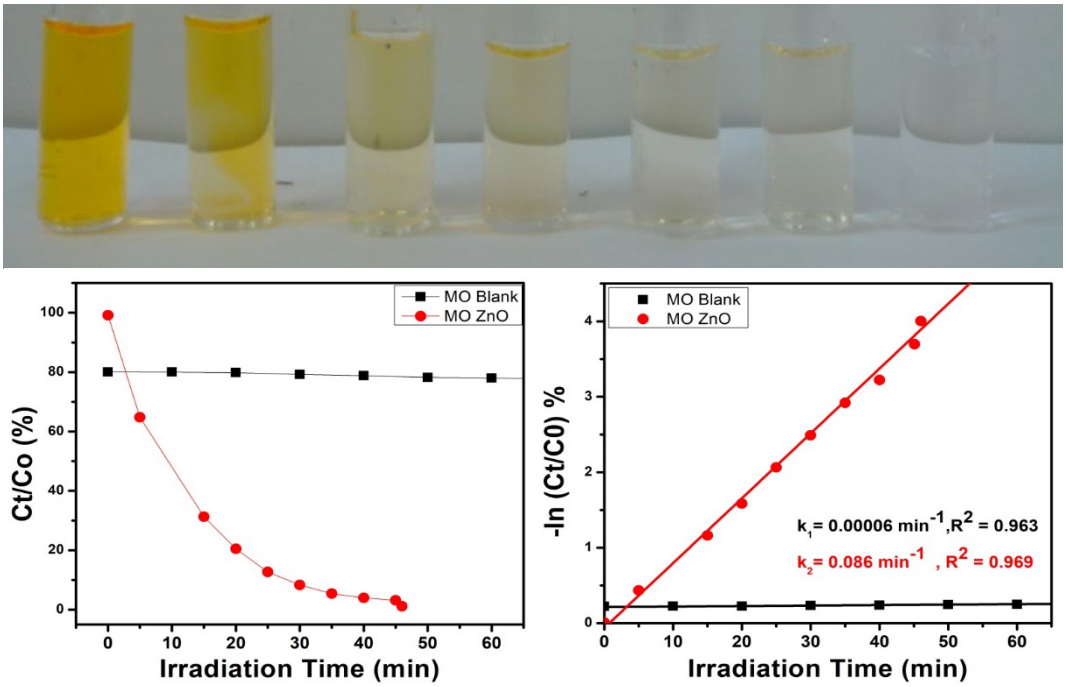

Fig. 7. Photocatalytic degradation of methylene orange (MO) dye blank and with ZnO nanorods (a) C_t/C_0 % (b) -ln (C_t/C_0) %.

3.5.2. Methylene blue degradation

The photodegradation of 15 uM (MB) spectra at room temperature with real-time degradation is shown in Figure 8. It is seen that the absorbance peaks of the blank (catalyst-free) MB are centered at around 670 nm and exhibit reducing behavior as exposure to radiation increases, with 90 percent degradation occurring in 60 minutes as shown in Figure (8-a). The photodegradation of MB solution containing ZnO nanorods serving as a photocatalyst is depicted in Figure 8 (b). Figure 8 (b) illustrates how the structures of MB in the existence of ZnO nanorods acting as a photocatalyst decline with increasing reaction time and disappear completely (99 %) after 20 minutes of UV exposure. Figure (8-c) illustrates the conclusion that MB dye degrades more quickly when ZnO nanorods are present as a photocatalyst than when MB blank is exposed to UV light.

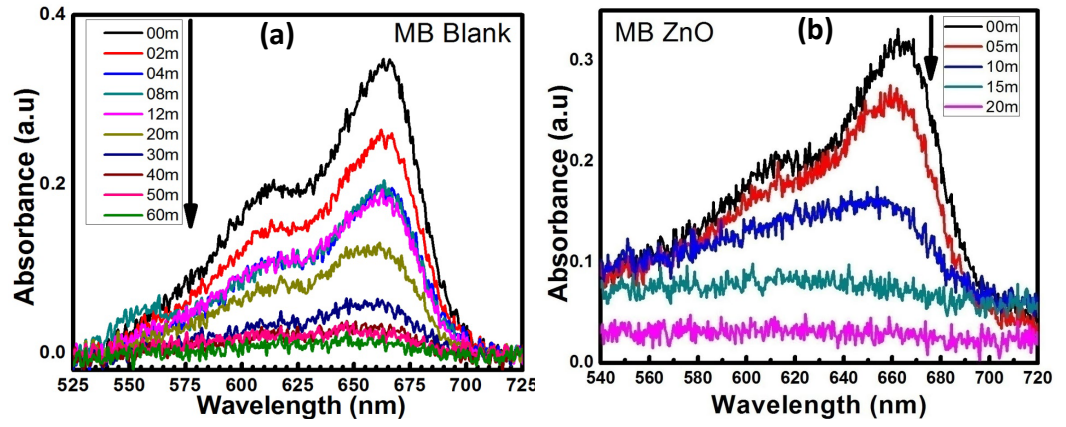

Fig. 8. UV-Vis spectra of photocatalytic degradation of methylene blue (MB) (a) blank (b) ZnO nanorods as a photocatalyst.

$$\ln C_0 / C_t = k_{MB}t \quad (5)$$

In the above equation, C_0 and C_t represent all the amounts of MB absorbed at 0 and 120-minute intervals of 10 minutes in the UV light. The letters t and k_{MB} represent the reaction's response time and rate constants. As shown in Figure (9-b), a tauc plot was used to evaluate the linear fitting versus the light exposure period of the photocatalytic breakdown of MB. Evaluating the slope of the related fitting curve yields the estimated kinetic degradation rate constant (k) for MB Blank and in the presence of ZnO nanorods as shown in Table 2. It seems that the ZnO nanorod sample has a high kinetic degradation rate constant of k=0.180 min-1 and a fast MB decomposition rate due to the abundance of charge carriers that facilitate a successful oxidation process under sunlight.

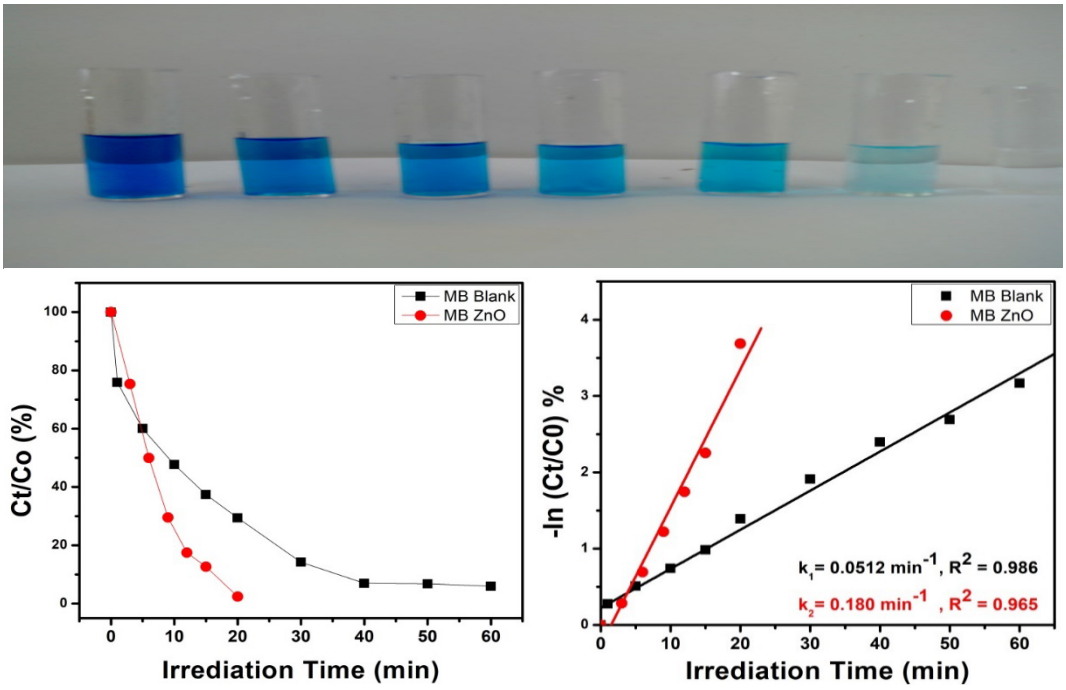

Fig. 9. photocatalytic degradation of Methylene Blue (MB) Blank and with ZnO nanorods (a) C_t/C_o (%) (b) –ln (C_t/C_0) %.

Table 2. Detailed photodegradation parameters of blank and ZnO nanorods. added MO & MB.

Dopant concentration	Rate constant	Residual concentration	Half-life of dye
w%	K (min^{-1})	(R^2)	$T_{1/2}$ (min)
MO Blank	0.00006	0.965	1.55×10^4
MO ZnO	0.086	0.969	8.03
MB Blank	0.051	0.986	13.5
MB ZnO	0.180	0.965	3.85

3.5.3. Photodegradation mechanism

A breakdown mechanism of the dyes examined in this study, MB, and MO, is shown in Figure-10. The attachment of the dye on the NRs' surface initiates the dye breakdown process because of their mutual attraction. Following their adsorption, the molecules are exposed to UV radiation with an energy larger than that of the band gap of the ZnO NRs (3.1–6.2) eV. This radiation causes an electron to be excited in the valence band (VB), and then go to the conduction band (CB), where it creates an electron-hole pair. When this happens, the holes engage with water molecules to produce radicals of hydroxyl (OH^-) while the electrons stimulated by light react to molecular oxygen (O^{-2}) to produce super oxygen radicals (O^{2*}). Since both the O^{2*} and OH^- radicals have extremely

high oxidation coefficients, when they come into contact with dye molecules, they trigger the original molecules to degrade and produce environment-friendly contaminants [59]. When MB is present at the surface of the ZnO NR's, the S atoms of the C − S+ = C group engage with the O^{2*} and OH^- radicals, reducing the C=N bond [60][61]. The next steps involve some demethylation and decolorization activities, which produce CO_2, H_2O, and a few mineral species as byproducts. However, the N=N link is broken first in the photocatalytic breakdown of MO, which results in the molecule's segregation [62]. After that, the radicals target the CH_3-N-CH_3 group, breaking down the CH_3 group [63]. After that, a few intermediary processes are carried out to release one of the aromatic rings and produce the ultimate residues, which include CO_2 and H_2O. A comparative study of the current work with similar research studies is mentioned in Table 3.

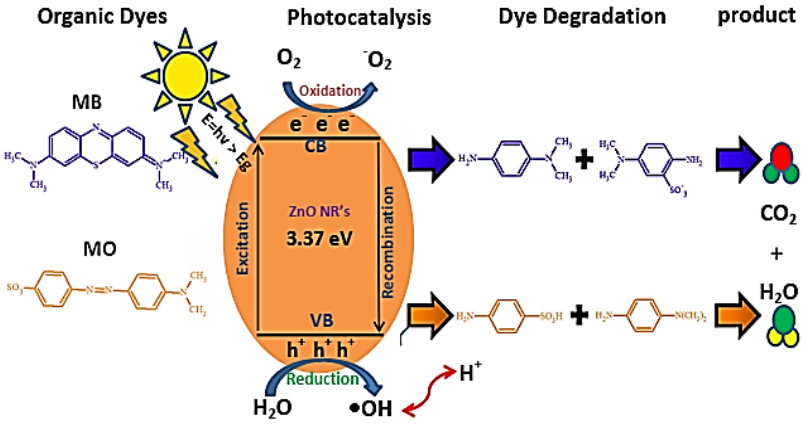

Fig. 10. Schematic illustration of the photocatalytic degradation of methylene blue (MB) and methyl orange (MO) in the presence of ZnO nanorods.

Table 3. A review of the relevant literature and a comparison of the current studies.

Photocatalyst	Organic (Dye)	Light Source	Rate Constant (min^{-1})	Exposure Time (min)	Photodegradation (%)	Reference
ZnO NP's	RhB	UV/Xenon	0.034	70	94	[64]
ZnO NR's	MB	Sun Simulator	0.013	45	75	[65]
ZnO NR's	MB	Sunlight	---------	150	93	[66]
ZnO NP's	MB	UV lamp 6W	---------	120	81	[67]
ZnO NR's	MB	UV lamp 500W	0.013	180	35	[67]
ZnO NR's	MB	UV/Xe 300W	0.180	20	99	(current work)
ZnO MR's	MO	UV/Xe 300W	0.086	46	99	(current work)

4. Conclusion

The high-efficiency photocatalyst ZnO nanorods are synthesized by utilizing a hydrothermal route of synthesis. Several characterization methods, including FESEM, XRD, FTIR, and UV vis spectroscopy, were used to verify the morphology, crystal structure, functional groups, and optical bandgap of the generated ZnO nanorods. It concludes that compared to several earlier

comparable assessments, the hydrothermally produced ZnO nanorod reveals a higher photodegradation efficiency for (MB & MO) dyes. In the presence of synthesized ZnO nanorods, the photodegradation efficiency for the elimination of MB was found to be 39.4% higher than that of MO dye. In conclusion, it has been demonstrated that ZnO is a more effective photocatalyst compared to a variety of other metal oxide semiconductors. It has been demonstrated that ZnO nanorods can quickly and economically eliminate organic substances like MB and MO from wastewater. From a long-term perspective, the photocatalytic performance of ZnO nanocrystals can be further improved by adding a certain noble or transition metal.

Declaration of interests

The authors declare that they have no known competing financial interests or personal relationships that could have appeared to influence the work reported in this paper.

Acknowledgments

The authors extend their appreciation to King Saud University, Saudi Arabia, for funding this work through Researchers Supporting Project number (RSP2024R397), King Saud University, Riyadh, Saudi Arabia.

References

[1] M. I. Sohail et al., 2019, pp. 1-54; https://doi.org/10.1016/bs.coac.2019.10.002

[2] M. Nasrollahzadeh, S. M. Sajadi, M. Sajjadi, Z. Issaabadi, 2019, pp. 113-143; https://doi.org/10.1016/B978-0-12-813586-0.00004-3

[3] S. Malik, K. Muhammad, Y. Waheed, Molecules, vol. 28, no. 2, p. 661, Jan. 2023; https://doi.org/10.3390/molecules28020661

[4] J. Lin et al., Nat. Rev. Earth Environ., vol. 4, no. 11, pp. 785-803, Oct. 2023; https://doi.org/10.1038/s43017-023-00489-8

[5] T. Islam, M. R. Repon, T. Islam, Z. Sarwar, M. M. Rahman, Environ. Sci. Pollut. Res., vol. 30, no. 4, pp. 9207-9242, Dec. 2022; https://doi.org/10.1007/s11356-022-24398-3

[6] S. Sudarshan et al., J. Appl. Microbiol., vol. 134, no. 2, Feb. 2023; https://doi.org/10.1093/jambio/lxac064

[7] M. Azad, G. Ali Khan, F. Ismail, W. Ahmed, Inorg. Chem. Commun., vol. 145, p. 109987, Nov. 2022; https://doi.org/10.1016/j.inoche.2022.109987

[8] Y. Ahmadi, K.-H. Kim, Renew. Sustain. Energy Rev., vol. 189, p. 113948, Jan. 2024; https://doi.org/10.1016/j.rser.2023.113948

[9] M. Baruah, S. L. Ezung, S. Sharma, U. Bora Sinha, D. Sinha, Inorg. Chem. Commun., vol. 144, p. 109905, Oct. 2022; https://doi.org/10.1016/j.inoche.2022.109905

[10] A. Mukherjee, N. Goswami, D. Dhak, Chem. Africa, vol. 6, no. 2, pp. 609-628, Apr. 2023; https://doi.org/10.1007/s42250-022-00467-5

[11] B. Pizzicato, S. Pacifico, D. Cayuela, G. Mijas, M. Riba-Moliner, Molecules, vol. 28, no. 16, p. 5954, Aug. 2023; https://doi.org/10.3390/molecules28165954

[12] R. H. Waghchaure, V. A. Adole, B. S. Jagdale, Inorg. Chem. Commun., vol. 143, p. 109764, Sep. 2022; https://doi.org/10.1016/j.inoche.2022.109764

[13] R. H. Waghchaure, P. B. Koli, V. A. Adole, B. S. Jagdale, Results Chem., vol. 4, Jan. 2022; https://doi.org/10.1016/j.rechem.2022.100488

[14] P. Kumari, A. Kumar, Results in Surfaces and Interfaces, vol. 11, p. 100122, May 2023; https://doi.org/10.1016/j.rsurfi.2023.100122

[15] M. D. Khan, A. Singh, M. Z. Khan, S. Tabraiz, J. Sheikh, J. Water Process Eng., vol. 53, p. 103579, Jul. 2023; https://doi.org/10.1016/j.jwpe.2023.103579

[16] S. Ledakowicz, K. Paździor, Molecules, vol. 26, no. 4, p. 870, Feb. 2021; https://doi.org/10.3390/molecules26040870

[17] G. Bal, A. Thakur, Mater. Today Proc., vol. 50, pp. 1575-1579, 2022; https://doi.org/10.1016/j.matpr.2021.09.119

[18] M. Rani, J. Yadav, U. Shanker, C. Wang, Environ. Sci. Pollut. Res., Feb. 2024; https://doi.org/10.1007/s11356-024-32455-2

[19] M. Bhattu, J. Singh, Chemosphere, vol. 321, p. 138072, Apr. 2023; https://doi.org/10.1016/j.chemosphere.2023.138072

[20] N. K. Hassan, M. A. Fakhri, A. W. Abdulwahhab, U. Hashim, Key Eng. Mater., vol. 911, pp. 55-64, Feb. 2022; https://doi.org/10.4028/p-8lgbrw

[21] A. U. Hasanah, P. L. Gareso, N. Rauf, D. Tahir, ChemBioEng Rev., vol. 10, no. 5, pp. 698-710, Oct. 2023; https://doi.org/10.1002/cben.202300004

[22] E. Daher, Design of Novel ZnO Nanostructures for Enhanced Photocatalytic Degradation of Organic Pollutants To cite this version : HAL Id : tel-04315851 Sorbonne Université Université Libanaise Conception de Nouvelles Nanostructures de ZnO pour une Dégradation Photo,2023.

[23] D. D. Thongam, H. Chaturvedi, Chemosphere, vol. 313, p. 137600, Feb. 2023; https://doi.org/10.1016/j.chemosphere.2022.137600

[24] S. Zhang, H. Zheng, P. G. Tratnyek, Nat. Water, vol. 1, no. 8, pp. 666-681, Jul. 2023; https://doi.org/10.1038/s44221-023-00098-1

[25] S. Mishra, B. Sundaram, Mater. Today Proc., Jul. 2023; https://doi.org/10.1016/j.matpr.2023.07.147

[26] H. Xie, F. Ding, H. Mu, Nanotechnology, vol. 30, no. 8, p. 085708, Feb. 2019; https://doi.org/10.1088/1361-6528/aaf197

[27] R. Devi, M. Bulla, S. Kumar, A. K. Mishra, V. Kumar, Advanced Functional Materials and Methods for Photodegradation of Toxic Pollutants, Elsevier, 2024, pp. 327-359; https://doi.org/10.1016/B978-0-323-95953-7.00015-1

[28] M. Shoeb et al., J. Phys. Chem. Solids, vol. 184, p. 111707, Jan. 2024; https://doi.org/10.1016/j.jpcs.2023.111707

[29] M. A. Al-Gharibi, H. H. Kyaw, J. N. Al-Sabahi, M. T. Zar Myint, Z. A. Al-Sharji, M. Z. Al-Abri, Mater. Sci. Semicond. Process., vol. 134, p. 105994, Nov. 2021; https://doi.org/10.1016/j.mssp.2021.105994

[30] N. Verma et al., J. Nanomater., vol. 2022, 2022; https://doi.org/10.1155/2022/7532332

[31] K. Mageswari, P. Prabukanthan, J. Madhavan, Environ. Sci. Pollut. Res., vol. 30, no. 14, pp. 40174-40188, Jan. 2023; https://doi.org/10.1007/s11356-022-25097-9

[32] S. Kanwal, M. Tahir Khan, V. Tirth, A. Algahtani, T. Al-Mughanam, A. Zaman, ACS Omega, vol. 8, no. 31, pp. 28749-28757, Aug. 2023; https://doi.org/10.1021/acsomega.3c03418

[33] F. del C. Gómez Torres et al., Boletín la Soc. Española Cerámica y Vidr., vol. 62, no. 4, pp. 348-356, Jul. 2023; https://doi.org/10.1016/j.bsecv.2022.05.004

[34] S. Patial et al., Environ. Res., vol. 197, p. 111134, Jun. 2021; https://doi.org/10.1016/j.envres.2021.111134

[35] R. B. Rashid, D. H. Hussain, R. S. Mahmood, J. Southwest Jiaotong Univ., vol. 55, no. 1, 2020; https://doi.org/10.35741/issn.0258-2724.55.1.53

[36] M. Gholami, H. Rasoulzadeh, T. Ahmadi, M. Hosseini, Mater. Lett., vol. 269, p. 127647, Jun. 2020; https://doi.org/10.1016/j.matlet.2020.127647

[37] O. Gultepe, F. Atay, Z. Dikmen, Mater. Chem. Phys., vol. 307, p. 128170, Oct. 2023; https://doi.org/10.1016/j.matchemphys.2023.128170

[38] N. Lal, K. Chawla, S. Sharma, D. K. Yadav, C. Lal, Orient. J. Chem., vol. 39, no. 1, pp. 136-143, Feb. 2023; https://doi.org/10.13005/ojc/390116

[39] R. Verma et al., Chem. Pap., vol. 77, no. 9, pp. 5587-5597, Sep. 2023; https://doi.org/10.1007/s11696-023-02831-2

[40] L. Nehru et al., Artif. Cells, Nanomedicine, Biotechnol., vol. 51, no. 1, pp. 318-333, Dec. 2023; https://doi.org/10.1080/21691401.2023.2232654

[41] M. L. Popa, M. D. Preda, I. A. Neacşu, A. M. Grumezescu, O. Ginghină, Int. J. Mol. Sci., vol. 24, no. 3, p. 1875, Jan. 2023; https://doi.org/10.3390/ijms24031875

[42] J. A. A. Abdullah, M. J. Rosado, A. Guerrero, A. Romero, New J. Chem., vol. 47, no. 9, pp. 4409-4417, 2023; https://doi.org/10.1039/D3NJ00131H

[43] A. Ejsmont, J. Goscianska, Materials (Basel)., vol. 16, no. 4, p. 1641, Feb. 2023; https://doi.org/10.3390/ma16041641

[44] N. Dogra, P. Agrawal, S. Pathak, R. Saini, S. Sharma, Int. J. Hydrogen Energy, vol. 48, no. 67, pp. 26210-26220, Aug. 2023; https://doi.org/10.1016/j.ijhydene.2023.03.352

[45] X. Zhang, L. Zhou, X. Tu, F. Hu, Polyhedron, vol. 246, p. 116668, Dec. 2023; https://doi.org/10.1016/j.poly.2023.116668

[46] S. Maghsoudi, R. Abdullah Mirzaie, M. Ghalkhani, A. Anaraki Firooz, J. Phys. Chem. Solids, vol. 176, p. 111269, May 2023; https://doi.org/10.1016/j.jpcs.2023.111269

[47] M. C. R. Silva et al., Molecules, vol. 29, no. 2, p. 391, Jan. 2024; https://doi.org/10.3390/molecules29020391

[48] T. M. Abdelghany et al., Biomass Convers. Biorefinery, vol. 13, no. 1, pp. 417-430, Jan. 2023; https://doi.org/10.1007/s13399-022-03412-1

[49] I. AmorBen et al., Biomass Convers. Biorefinery, Sep. 2023; https://doi.org/10.1007/s13399-023-04923-1

[50] T. Chitradevi, A. Jestin Lenus, N. Victor Jaya, Mater. Res. Express, vol. 7, no. 1, p. 015011, Jan. 2020; https://doi.org/10.1088/2053-1591/ab5c53

[51] B. Ben Seghir et al., Nanomaterials, vol. 13, no. 17, p. 2425, Aug. 2023; https://doi.org/10.3390/nano13172425

[52] R. Ishwarya et al., J. Drug Deliv. Sci. Technol., vol. 79, p. 104002, Jan. 2023; https://doi.org/10.1016/j.jddst.2022.104002

[53] M. S, H. N, V. P.P, Bionanoscience, vol. 10, no. 1, pp. 112-121, Mar. 2020; https://doi.org/10.1007/s12668-019-00698-w

[54] A. M. El-Khawaga et al., Biomass Convers. Biorefinery, Sep. 2023; https://doi.org/10.1007/s13399-023-04827-0

[55] R. S. Dangana, R. C. George, F. K. Agboola, Green Chem. Lett. Rev., vol. 16, no. 1, Jan. 2023; https://doi.org/10.1080/17518253.2023.2169591

[56] L. Bai et al., Arab. J. Chem., vol. 16, no. 3, p. 104523, Mar. 2023; https://doi.org/10.1016/j.arabjc.2022.104523

[57] S. Rajamanickam, S. M. Mohammad, I. A. Razak, A. Muhammad, S. M. Abed, Mater. Res. Bull., vol. 161, p. 112148, May 2023; https://doi.org/10.1016/j.materresbull.2023.112148

[58] R. Li, M. Li, X. Wu, H. Yu, R. Jin, J. Liang, Mater. Des., vol. 225, p. 111583, Jan. 2023; https://doi.org/10.1016/j.matdes.2022.111583

[59] S. A. Al-Zahrani, A. M. Khedr, A. M. Alturki, W. S. Abo El-Yazeed, J. Mol. Liq., vol. 395, p. 123956, Feb. 2024; https://doi.org/10.1016/j.molliq.2024.123956

[60] P. A. Luque-Morales et al., Materials (Basel)., vol. 14, no. 24, 2021; https://doi.org/10.3390/ma14247537

[61] F. Yu et al., J. Alloys Compd., vol. 982, p. 173756, Apr. 2024; https://doi.org/10.1016/j.jallcom.2024.173756

[62] M. Muduli, M. Choudhary, V. Sonpal, S. Ray, Sustain. Water Resour. Manag., vol. 9, no. 6, p. 186, Dec. 2023; https://doi.org/10.1007/s40899-023-00975-3

[63] A. M. Nasir et al., J. Water Process Eng., vol. 40, p. 101878, Apr. 2021; https://doi.org/10.1016/j.jwpe.2020.101878

[64] Q. I. Rahman, M. Ahmad, S. K. Misra, M. Lohani, Mater. Lett., vol. 91, pp. 170-174, Jan. 2013; https://doi.org/10.1016/j.matlet.2012.09.044

[65] B. Park, Under Visible Light Irradiation, vol. 1, no. 858, 2022.

[66] P. Dash, A. Manna, N. C. Mishra, S. Varma, Phys. E Low-dimensional Syst. Nanostructures, vol. 107, pp. 38-46, Mar. 2019; https://doi.org/10.1016/j.physe.2018.11.007

[67] S. Modi et al., Water, vol. 15, no. 12, p. 2275, Jun. 2023; https://doi.org/10.3390/w15122275